Precision measurement of the branching fractions of the $5p\,^2P_{1/2}$ state in $^{88}Sr^+$ with a single ion in a microfabricated surface trap

Jean-Pierre Likforman, Vincent Tugayé,* Samuel Guibal, and Luca Guidoni†
Université Paris-Diderot, Sorbonne Paris Cité, Laboratoire Matériaux et Phénomènes Quantiques, UMR 7162 Centre National de la Recherche Scientifique, F-75205 Paris, France
(Received 24 November 2015; revised manuscript received 29 March 2016; published 10 May 2016)

We measured the branching fractions for the decay of the $5p\,^2P_{1/2}$ state of $^{88}Sr^+$ by applying a recently demonstrated photon-counting sequential method [M. Ramm, T. Pruttivarasin, M. Kokish, I. Talukdar, and H. Häffner, Phys. Rev. Lett. **111**, 023004 (2013)] to a single ion laser cooled in a microfabricated surface trap. The branching fraction for the decay into the $5s\,^2S_{1/2}$ ground level was found to be $p = 0.9449(5)$. This result is in good agreement with recent theoretical calculations but disagrees with previous experimental measurements, however affected by a one-order-of-magnitude larger uncertainty. This experiment demonstrates that microtrap technology is also applicable in the domain of precision measurements and spectroscopy.

DOI: 10.1103/PhysRevA.93.052507

I. INTRODUCTION

Atomic spectroscopy data provide, from a historical point of view, one of the most important experimental inputs that triggered the development of quantum mechanics (e.g., Ängström measurements of Balmer series of the hydrogen atom). Later on, precision measurements of the characteristic features of atomic transitions (i.e., transition frequencies, levels lifetimes, and branching fractions) allowed for the development of theoretical methods that now aim at a complete understanding of atomic level structures, at least in the simpler cases [1]. The comparison between theory and experiments is then necessary to test these models that are essential for addressing some fundamental questions like parity nonconservation or the search for the electron electric dipole moment [2]. Precise knowledge of atomic properties is also very important for astronomical and cosmological studies [3] in which easily identified atomic lines give precious information about celestial objects. Finally, the advent of optical clocks (that display improved performances with respect to atomic microwave clocks that define the time unit) [4] requires precise models in order to obtain reliable evaluations of systematic frequency shifts that affect accuracy (e.g., blackbody radiation shift [5]). In the case of alkaline-earth elements, the singly ionized state is particularly interesting because theoretical calculations are more precise in the presence of a single valence electron. Singly ionized alkaline-earth elements are also a system of choice for trapped ion based quantum information experiments [6] and are among the species used for precision clocks [4]. Therefore, several experimental techniques have been developed that allow for internal and motional quantum state control [6–8]. By restricting ourselves to the case of heavier alkaline-earth elements (i.e., species with D metastable states), these techniques have been recently applied to obtain precision measurements of spectroscopical quantities on laser-cooled $^{40}Ca^+$ ions [9–12], $^{138}Ba^+$ ions [13–15], and $^{88}Sr^+$ ions [16–19]. In this paper we present the precision measurement of the branching fractions for the decay of the $5p\,^2P_{1/2}$ state of $^{88}Sr^+$. In particular, we measured the probability p and $1-p$ for the decay of the $5p\,^2P_{1/2}$ to the $5s\,^2S_{1/2}$ and $4d\,^2D_{3/2}$ states to be, respectively, $p = 0.9449(5)$ and $1-p = 0.0551(5)$. This result can also be expressed in terms of branching ratio $B = \frac{p}{1-p}$ as $B = 17.14(16)$, affected by a fractional uncertainty of 1×10^{-2}.

Experimental spectroscopy concerning Sr ions has been addressed in several papers, the results of which are compiled in the reference [20]. The experimental transition probabilities A_{SP} and A_{PD} for the $5s\,^2S_{1/2} \rightarrow 5p\,^2P_{1/2}$ ($\nu = 711$ THz, $\lambda = 422$ nm) and $4d\,^2D_{3/2} \rightarrow 5p\,^2P_{1/2}$ ($\nu = 275$ THz, $\lambda = 1092$ nm) transitions listed in this compilation (and in the NIST database [21]) are obtained taking into account measurements of the branching fractions and of the lifetime $\tau_{P_{1/2}}$. Lifetime and branching fractions of the $^{88}Sr^+$ $5p\,^2P_{1/2}$ level were measured in 1967 by Gallagher in an Argon discharge by Hanle-effect spectroscopy [22]. The lifetime of the $5p\,^2P_{1/2}$ level was later measured with increased precision with the fast ion-beam technique [23,24]. The NIST database is then based on the two measurements $B = 13.4(2.0)$ [22] and $\tau_{P_{1/2}} = 7.39(7)$ ns [24]. A more recent, albeit quite indirect, experimental measurement of A_{SP} is also given in Ref. [25].

Theoretical works on $^{88}Sr^+$ are largely motivated by the use the dipole-forbidden "clock" $5s\,^2S_{1/2} \rightarrow 4d\,^2D_{5/2}$ Sr^+ transition ($\nu = 446$ THz, $\lambda = 674$ nm) as a secondary frequency standard [16,17,26]. Indeed, in 2006 the International Committee for Weights and Measures included this transition among the recommended secondary representation of the second [27]. The need of exactitude, proper to frequency standards, enforces the accurate calculation of blackbody frequency shift. In order to calculate such a shift, precise determinations of dipole moments of low-lying transition are needed. Such kinds of calculations for $^{88}Sr^+$ have been performed with increasing precision during recent years [28–32]. Several of these results are resumed and compared in Ref. [5]. Another theoretical calculation of dipole moments can be found in a more recent paper devoted to the estimation of parity nonconservation effects in $^{87}Sr^+$ and $^{137}Ba^+$ [33].

The paper is organized as follows. In Sec. II we present the experimental setup and give some details concerning

*Also at Département de Physique, Ecole Normale Supérieure de Lyon, Université de Lyon, 46 Avenue d'Italie, F-69364 Lyon, France.
†luca.guidoni@univ-paris-diderot.fr

the surface trap and the implementation of the sequential method. We present the results in Sec. III, and we discuss the systematic errors and describe the techniques used to determine their contributions to the final result. Finally, in Sec. IV we compare the result to the literature and briefly discuss possible improvements.

II. EXPERIMENTAL METHODS

A. Trapping, cooling, and laser locking

The experiments are based on a symmetric five-wires surface trap [34] with a nominal ion-surface distance $d = 110\,\mu$m (see Fig. 1). The original purpose of this trap is the study of the anomalous heating problem and it is optimized for single-ion operation. The trap is microfabricated in a cleanroom with standard photolithographic techniques on a silica substrate. The 5-μm-thick gold electrodes are obtained by electroplating [35] with an interelectrode distance of 5 μm in the central region of the trap. The chip is glued on a ceramic holder and bonded with 20-μm-diameter gold wires. Filtered static voltages (dc) provided by a DAC computer card (Measurement Computing PCI-DAS) feed the ceramic holder through *in vacuo* screened kapton wires. The trap is driven with a radio-frequency (rf) voltage amplitude $V_{\rm rf} \sim 150$ V at a frequency of 33.2 MHz and typically displays radial frequencies in the 1.5–2-MHz range and an axial frequency of $\simeq$200 kHz for Sr^+. The trapping potential is tailored (e.g., tilted) by the application of a set of static voltages to the dc electrodes calculated with the matrix approach developed in Ref. [35]. The matrix is derived by the analytical calculation of the electrostatic potential generated by each electrode [36]. The stray electric fields are compensated for using a rf correlation technique [37] adapted to surface traps [35]. We estimate the uncompensated excess micromotion amplitude considering that the sensitivity for a null position is 1 V/m along the transverse direction parallel to the trap surface and 25 V/m in the direction orthogonal to the trap. The corresponding excess micromotion amplitudes are 1 and 12 nm along the parallel and orthogonal directions, respectively (in terms of peak velocity components 0.2 and 2.5 m/s, respectively). Micromotion is neither expected nor detected along the trap axis.

Sr^+ ions are loaded from an oven containing a strontium dendrite (Aldrich, 99.9% pure). Neutral atoms are ionized by driving a two-photon transition towards a self-ionizing level [38]. The photoionizing laser pulses are issued from a frequency doubled Ti:sapphire oscillator (Tsunami, Spectra-Physics) with a central frequency of 695 THz ($\lambda = 431$ nm) and a pulse duration of $\simeq$100 fs.

Single trapped $^{88}Sr^+$ ions are Doppler cooled using the 711-THz $5s\,^2S_{1/2} \rightarrow 5p\,^2P_{1/2}$ optical transition (see Fig. 2). This transition is driven using laser light generated by a commercial extended-cavity GaN laser diode (Toptica DL100). The laser frequency is locked to an atomic reference, taking advantage of the near coincidence ($\nu_{Sr^+} - \nu_{Rb} \simeq 440$ MHz) between the $^{88}Sr^+\,5s\,^2S_{1/2} \rightarrow 5p\,^2P_{1/2}$ and the ^{85}Rb $5s\,^2S_{1/2}(F = 2) \rightarrow 6p\,^2P_{1/2}(F' = 3)$ transitions [39]. The 710 962 401 328(40)-kHz absolute frequency of this ^{85}Rb transition has been recently measured by the frequency-comb technique [40]. The electronic signal for laser locking is obtained using a saturated-absorption setup, based on a rubidium cell heated to 100° C. The detuning of the cooling beam with respect to the $5s\,^2S_{1/2} \rightarrow 5p\,^2P_{1/2}$ transition is controlled using an acousto-optic modulator (AOM) in a double-pass geometry driven at a frequency around 220 MHz. Disregarding the power used for frequency and intensity stabilization, up to 500 μW are available at the output of a single-mode polarization-maintaining optical fiber.

A commercial fiber laser (Koheras Adjustik Y10) drives the $4d\,^2D_{3/2} \rightarrow 5p\,^2P_{1/2}$ 275-THz "repumping" transition (see

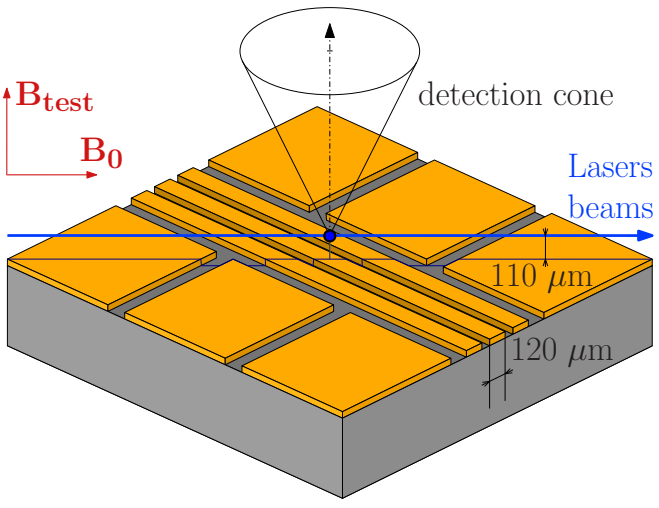

FIG. 1. Schematic view of the surface ion trap. Cooling, repumping, and photoionizing laser beams propagate parallel to the trap surface aligned at 45° with respect to the trap axis. During normal operation, a magnetic field $\mathbf{B_0}$ of the order of 1×10^{-4} T defines a quantization axis parallel to the propagation direction of laser beams. While testing systematic effects possibly induced by polarization sensitivity in the detection chain, the magnetic field ($B_{\rm test}$) has the same amplitude as $\mathbf{B_0}$ but its direction is orthogonal to the trap surface.

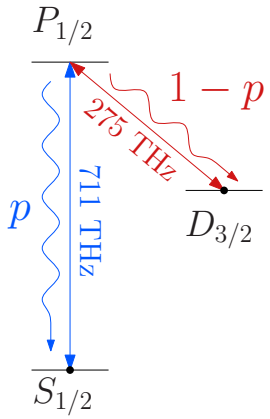

FIG. 2. Low-energy levels of $^{88}Sr^+$. Two laser sources are used to produce fluorescence cycles of $^{88}Sr^+$: a cooling laser at 711 THz (421.7 nm) and a repumping laser at 275 THz (1092 nm). Starting in the $5p\,^2P_{1/2}$ energy level, the electronic excitation can relax either to the ground state (with a probability p) or to the metastable state $4d\,^2D_{3/2}$ (with probability $1 - p$).

Fig. 2) to avoid the accumulation of the ions into the metastable $4d\,^2D_{3/2}$ state during the cooling process. This laser has a nominal linewidth of 70 kHz and is stabilized against long-term drifts by a transfer-lock technique using a scanning ring cavity referenced to the stabilized 711-THz laser diode [41,42]. The feedback loop of the lock is, in our case, relatively slow (bandwidth $\simeq$3 Hz) [43].

During normal operation a magnetic field $\mathbf{B_0}$ with a magnitude of the order of 1×10^{-4} T defines a quantization axis parallel to the substrate making an angle of 45° with the trap axis. The repumping and cooling laser beams propagate along this quantification axis and their linear polarization is parallel to the trap surface (see Fig. 1). This configuration prevents the ions from being optically pumped into a metastable dark state by the repumping laser alone [44].

Spontaneously emitted 711-THz ("blue") photons are collected by a large-aperture pair of achromatic lenses (Thorlabs AC508-075-A), spatially filtered with a 150-μm-diameter pinhole, spectrally filtered by an interference filter (Thorlabs FB420-10, 10-nm bandwidth) and detected by a photon-counting photomultiplier head (PMT). We used two different PMT heads in distinct experimental runs (Hamamatsu model H7828 or H10682-210). The measured global detection efficiency ϵ of the setup is $\epsilon \simeq 1.0 \times 10^{-3}$ with the first head and $\epsilon \simeq 1.4 \times 10^{-3}$ with the second head (see below for the description of the measurement technique). The logical pulses at the output of the detector are counted and accumulated by a stand alone microcontroller-based gated counter and transferred to the computer that controls the experiment.

Laser beams impinging on the ion are switched on and off using AOMs in a double-pass geometry driven through rf switches (Mini-Circuits ZYSWA-2-50DR) and then injected in single mode polarization maintaining optical fibers. The measured characteristic switching times for the cooling and repumping beams are shorter than 20 and 80 ns, respectively. A better than -77-dB extinction ratio has been measured on the repumping beam using a lock-in amplifier: as discussed below such a figure is of importance for the estimate of systematic errors. The intensity of the two laser beams impinging on the ion is actively stabilized as described below. At the output of each optical fiber the beam passes through a polarizer and is then sampled by a beam splitter and measured by a photodetector. A gateable servo loop with 10-kHz bandwidth acts on the rf amplitude that drives the AOM in order to keep the measured intensity constant (residual fluctuation smaller than 5%). Active intensity stabilization allows us to improve the control on resonant Rabi frequencies Ω_1 and Ω_2 associated to cooling and repumping beams, respectively. As explained below, resonant Rabi frequencies, together with respective detunings δ_1 and δ_2, determine the time evolution of the atomic density matrix. In particular, the knowledge of these experimental parameters is needed in order to evaluate systematic errors. We evaluate the resonant Rabi frequencies of cooling and repumping beams by analyzing a fluorescence spectrum obtained in a sequential way, similar to the technique described in Ref. [45]. In particular we scan a probe beam at 711 THz in the presence of the repumping beam at 275 THz slightly detuned with respect to the resonance ($\delta_2 \simeq 0$). In this situation several dark resonances are present in the spectrum [46] that contain information about the parameters of both lasers. The acquired spectrum is then fitted with the solution of optical Bloch equations (OBEs, see below) that allows us to retrieve four free parameters: $\Omega_1, \Omega_2, \delta_2$, and the magnetic field magnitude. For this analysis, the measurement of the collection efficiency ϵ helps to reduce uncertainties on the determinations of Rabi frequencies. The details of this spectroscopic technique, beyond the scope of this paper, will be given elsewhere. Please note that δ_2 is shifted to $\delta_2 \simeq 2\pi \times 80$ MHz during the measurement of branching fractions. A fully automated procedure is able to detect an ion loss during the data acquisition: in this case a new ion is automatically reloaded. This procedure allowed us to compress the effective time needed in order to achieve a low statistical uncertainty.

B. Sequential acquisition

We use a sequential technique largely inspired by the one applied for the first time by Ramm and coworkers in order to measure the branching fractions of the $4p\,^2P_{1/2}$ state in $^{40}Ca^+$ [11]. The same principle has been used more recently for the measurement of branching fractions of the $6p\,^2P_{1/2}$ state in $^{138}Ba^+$ [15]. The main differences here, apart from the ion species, are the single-ion operation and the trap technology (microfabricated surface trap versus mechanically assembled macrotraps) that are adopted for practical reasons. Briefly, in our experiment a single $^{88}Sr^+$ ion is first Doppler cooled and then prepared in the ground state by switching off the cooling beam while the repumping beam stays on.

A first counting window is then opened during which the cooling beam drives the $5s\,^2S_{1/2} \rightarrow 5p\,^2P_{1/2}$ transition in the absence of the repumping beam. In this phase the ion should scatter an average number of N_b blue photons ending up in the $4d\,^2D_{3/2}$ long-lived metastable state [lifetime $\tau_D = 435(4)$ ms [47]]. A second counting window is then opened during which the repumping beam drives the $4d\,^2D_{3/2} \rightarrow 5p\,^2P_{1/2}$ transition in the absence of the cooling beam. In this phase the ion should scatter a single $N_r = 1$ blue photon ending up in the ground state, closing in this way a detection loop. In the absence of photon losses (i.e., for a perfect detection efficiency $\epsilon = 1$) the probability p $(1-p)$ for the decay of the $5p\,^2P_{1/2}$ to the $5s\,^2S_{1/2}$ $(4d\,^2D_{3/2})$ state is obtained by measuring $\frac{N_b}{N_b+N_r}$ $(\frac{N_r}{N_b+N_r})$. This relationship still holds in case of imperfect collection efficiency ($\epsilon < 1$) because the correction is a common-mode factor for both measurements (e.g., $\frac{\epsilon N_b}{\epsilon N_b+\epsilon N_r} \equiv \frac{N_b}{N_b+N_r}$). The method is based on the assumption that this behavior is quite robust against variations of experimental conditions (e.g., Rabi frequencies drifts) [11]. Repeated counts of the number of scattered photons during the counting windows and an independent measurement of the background counts N_b^B and N_r^B associated to each phase (laser photons scattered by trap surfaces, residual ambient light, and photodetector dark counts) allow for the measurement of the branching fractions. Without considering the systematic effects, the uncertainty is dominated by the statistical error on N_r. A typical chronogram used in the experiment is represented in Fig. 3. In an experiment we acquire many bunches consisting of several hundred sequential acquisitions of N_b and N_r together with the measurements of corresponding backgrounds and we transfer the corresponding

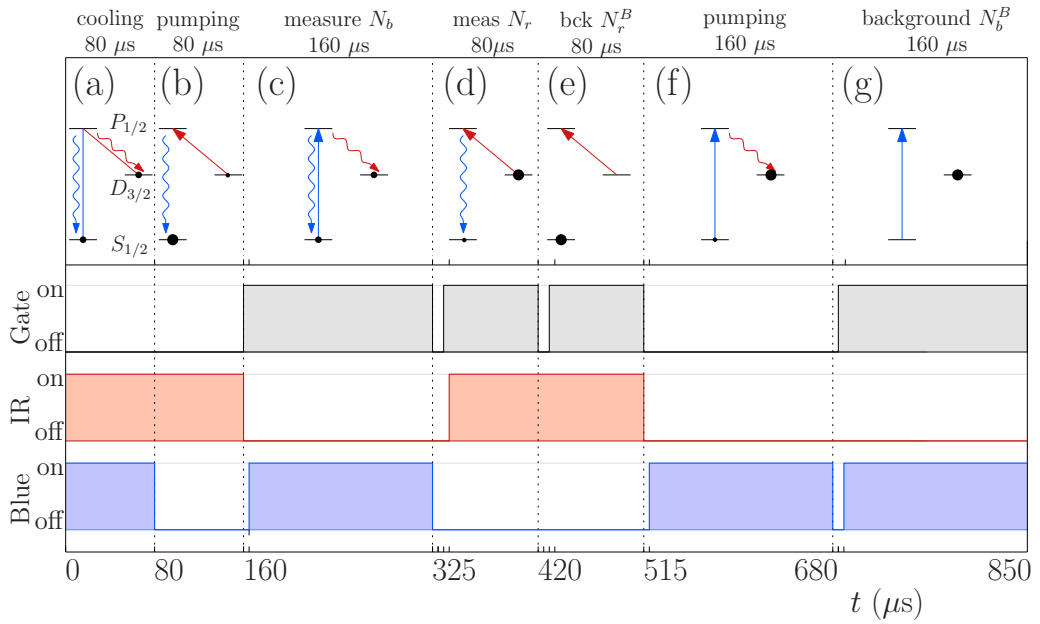

FIG. 3. Typical acquisition sequence used in a single detection cycle. (a) Laser cooling (80 μs, both lasers turned on). (b) Optical pumping in the ground state (80 μs, 711-THz laser turned off). (c) Measurement of N_b blue photons (160 μs, 711-THz laser turned on, 275-THz laser turned off). (d) Measurement of N_r blue photons (80 μs, 711-THz laser turned off, 275-THz laser turned on). (e) Measurement of the background signal N_r^B associated with phase (d) (80 μs, 711-THz laser turned off, 275-THz laser turned on). (f) Optical pumping in the metastable $4d\,^2D_{3/2}$ state to prepare the measurement of the background signal N_b^B associated with phase (c) (160 μs, 711-THz laser turned on, 275-THz laser turned off). (g) Measurement of the background signal N_b^B associated with phase (c) (160 μs, 711-THz laser turned on, 275-THz laser turned off). This sequence of duration 850 μs is typically repeated $\simeq 50 \times 10^6$ times. This sequence has been used for the third acquisition run (see Sec. III).

sums of detected photons to the computer. We checked that the measured averaged pulse durations associated to a chronogram are nominal (i.e., identical to the programed value) within the resolution of the instrument we used (± 4 ns, with a Tektronix 3032B oscilloscope, 300-MHz bandwidth). The amplitude of the time jitter associated to the pulses is lower than 40 ns.

III. RESULTS

A typical acquisition run consists of $\geq 50 \times 10^6$ sequence cycles that correspond to a "net" acquisition time of the order of 15–20 h. We performed three such runs with different Rabi frequencies and timings in order to check experimentally the estimations of systematics that are based on the resolution of optical Bloch equations, as explained below. The first acquisition run was based on a sequence with a N_b counting window of 80 μs and we used a H7828 PMT. The raw results of the first acquisition (sum of all detected photons in 54 272 970 cycles) are $N_b = 1\,295\,709, N_r = 105\,439, N_b^B = 342\,349$, and $N_r^B = 50\,418$. In the second acquisition run we increased the N_b counting window up to 160 μs, still using H7828 PMT. The raw results for the second run of 111 200 000 cycles are $N_b = 3\,521\,973, N_r = 244\,082, N_b^B = 1\,657\,903$, and $N_r^B = 136\,141$. The third acquisition run used an optimized timing for the sequence (with respect to systematic errors presented below) and a photon counter with increased performances (Hamamatsu H10682-210, with higher quantum efficiency and shorter dark time). The time windows of this sequence are those shown in Fig. 3. The raw results for the third run of 63 400 000 cycles are $N_b = 2\,844\,886, N_r = 93\,465, N_b^B = 1\,368\,075$, and $N_r^B = 7292$. Without taking into account the systematic effects (see below) and assuming a Poisson statistics for the photon counting these results give $p = 0.9454(6)\,[B = 17.33(20)]$, $p = 0.9453(5)\,[B = 17.27(17)]$, and $p = 0.9449(3)\,[B = 17.14(11)]$ for the first, second, and third run, respectively. Let us note that these three results are mutually compatible. The acquisitions also allow for the evaluation of the average detection efficiency of the setup: we obtained $\epsilon = 1.01 \times 10^{-3}$ for the first run, $\epsilon = 0.97 \times 10^{-3}$ for the second run, and $\epsilon = 1.36 \times 10^{-3}$ for the third run.

Systematic effects

Several systematic effects may affect the raw results presented above.

We consider first the residual birefringence of the detection chain that could induce a polarization-sensitive detection efficiency altering the isotropic behavior of the $5s\,^2S_{1/2} \rightarrow 5p\,^2P_{1/2}$ transition [11]. This effect can be estimated by repeating the experiment with a different orientation of magnetic field in order to evaluate it at the level of the statistical uncertainty of the final result. We acquired the same amount of data in the same condition as the first run with a magnetic field $\mathbf{B_{test}}$ which has the same magnitude as $\mathbf{B_0}$ but is orthogonal to the trap plane (see Fig. 1). This orientation of the quantification axis allows us to test the detection direction along which, according to the emission diagram of a $J = 1/2 \rightarrow J' = 1/2$ transition [48], we expect a maximum of sensibility to a possible polarization unbalance of emitted

photons. The raw results are in this case $N_b = 1\,671\,954, N_r = 114\,967, N_b^B = 478\,305$, and $N_r^B = 46\,035$, which give $p = 0.9454(5)$, perfectly compatible with the results obtained with an orthogonal orientation of magnetic field. We can therefore put an upper limit of 5×10^{-4} to this effect, in terms of uncertainty on p.

Collisions and off-resonant excitations of the $4d\,^2D_{5/2}$ long-lived metastable state can also be a source of systematic shifts. In order to evaluate these effects we performed a detailed study of collision events in our experimental setup [9]. As detailed below, these phenomena show up either as a permanent loss of the ion or as a reversible loss of fluorescence that can be measured during the cooling phase. The finite lifetime of the ion in the trap (permanent loss) does not affect directly the measurements because we filter out the acquisitions in which the ion is not present. On the other hand the events displaying a reversible loss of fluorescence may induce a systematic shift. Let us first remark that the data acquired during an integer number of whole cycles in the absence of fluorescence do not shift the value of p: these data correspond to a detection efficiency $\epsilon = 0$ and as long as a N_r cycle is coupled to a N_b cycle the value of p is unaffected by ϵ. However, each reversible collision event can unbalance two acquisition cycles: first when the ion "disappears" and then when it "reappears." The upper limit of the systematic shift induced by this phenomenon can be estimated by assuming that a maximum unbalance is produced for each collision: no counts during an acquisition phase (e.g., N_r) and a maximal excess count in the corresponding background phase (e.g., N_r^B). Considering this the "worst case" assumption, the knowledge of collision rates (see below) allows us to evaluate this upper limit to the systematic shift: in terms of p this shift is bounded by 10^{-7} (see Table I).

In order to characterize the collisions in our trap we followed a method similar to that exposed in Ref. [9]: we recorded the fluorescence of a single ion during a total time of 43 h with time bins of 5 ms. A first result of this study is a measurement of the lifetime of the cooled ion in the trap. Without taking into account extrinsic events (e.g., delocking of a laser frequency or accidental switching off), we had to reload a total number of 99 ions, which gives an average lifetime of 1560 s. The distribution of observed lifetimes is compatible with an exponential distribution. During the total acquisition time we also observed events displaying an abrupt disappearance of the fluorescence that is later recovered also abruptly. Following Ref. [9] it is possible to attribute these events to two kinds of phenomena depending on their duration. In a first case, nonresonant optical pumping and/or fine-structure-changing collisions can bring the ion in the $4d\,^2D_{5/2}$ state. These events should display a duration distributed exponentially with the lifetime $\tau_{D_{5/2}} = 390.8$ ms of the $4d\,^2D_{5/2}$ state [18]. On the other hand, some of the very short dark periods are likely to be the consequence of smaller perturbations by large impact-parameter collisions. This interpretation is supported by the analysis of the histogram of the time durations of the events reported in Fig. 4, in which the two classes of events clearly separate into one fraction following an exponential distribution characterized by $\tau_{D_{5/2}}$ (the lifetime is not an adjustable parameter for the fit displayed with a continuous line) and another fraction, accumulated around the origin, that contributes for 54% of the events. Let us note that the average time that separates these events (1800 and 1520 s for the long- and short-lived events, respectively) is of the same order of magnitude as what has been observed by Barton and coworkers under similar pressure conditions [9]. Contrary to the case of Ref. [9], we do not observe events displaying gradual reappearance of the fluorescence (within our resolution). A possible explanation of this behavior resides in the the lower depth of the pseudopotential well in our surface trap. This characteristic may not allow an ion that reaches

TABLE I. Systematic errors estimations on the branching fraction p calculated using the solutions of the OBE that describe the time evolution of the atomic density matrix during an acquisition sequence as a function of experimentally determined parameters (i.e., driving lasers parameters with nominal values $\Omega_1 = 2\pi \times 8.7$ MHz, $\Omega_2 = 2\pi \times 18$ MHz, $\delta_1 = -2\pi \times 27.5$ MHz, $\delta_2 = 2\pi \times 80$ MHz, and $B = 10^{-4}$ T). The uncertainties on the systematic errors are calculated considering a (conservative) $^{+20\%}_{-20\%}$ uncertainty on Rabi frequencies. The measured value for the dead time of the photodetection chain is used ($\tau_{PM} = 30 \pm 2$ ns).

Effect	Systematic shift on p	
Collisions	$<1 \times 10^{-7}$	
PM dead time	4.3×10^{-6}	$+1.8 \times 10^{-6}$
		-1.5×10^{-6}
$D_{3/2}$ lifetime and	0.4×10^{-6}	-0.4×10^{-6}
finite windows		$+1.9 \times 10^{-6}$
Laser leaks	1×10^{-8}	$\pm 1 \times 10^{-8}$
Timing precision	0	$\pm 2 \times 10^{-6}$
Total	5×10^{-6}	$+4 \times 10^{-6}$
		-3×10^{-6}

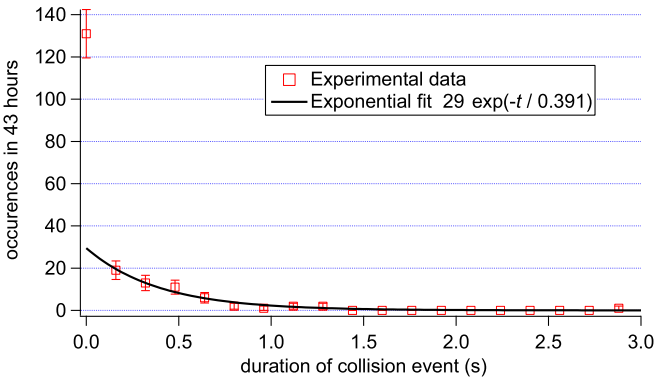

FIG. 4. Histogram of time durations of collision events observed during 43 h of operation in the surface trap. Each event is characterized by an abrupt disappearance of the fluorescence that reappears later in time. The fluorescence is acquired with an integration time of 5 ms and, within this resolution, the reappearance of the fluorescence is also abrupt. The solid line is a fit of the experimental data (with the exclusion of the shortest time bin of the histogram) with an exponential distribution characterized by an imposed decay time $\tau_{D_{5/2}} = 390.8$ ms (fixed parameter) and an amplitude on the first bin (adjustable parameter) of 29 events. The statistical weights of the populations associated to the two classes in this bimodal histogram are 54% for the short-lived events and 46% for the exponentially distributed events, respectively.

high temperatures to stay trapped and be recooled with long characteristic times.

Other systematic effects arise from the dead time of the photomultiplier, the finite lifetime of the $4d\,^2D_{3/2}$ state, the finiteness of the durations of acquisition windows, and the finiteness of the extinction ratio of AOM switching. All these effects can be evaluated by solving the OBE that describe the time evolution of the atomic density matrix during an acquisition sequence as a function of driving lasers parameters (i.e., $\Omega_1,\Omega_2,\delta_1,\delta_2$ as defined in Sec. I, where the indices 1 and 2 refer to the cooling and repumping laser, respectively). We numerically solve the OBE including all the Zeeman sublevels involved in the experiment (i.e., eight sublevels) and taking into account the effect of magnetic field B and laser polarizations. This multilevel approach allows us to better estimate the characteristic times associated to optical pumping in the experimental conditions. The nominal driving lasers parameters (measured in the experiment) are $\Omega_1 = 2\pi \times 8.7\,\text{MHz}$, $\Omega_2 = 2\pi \times 18\,\text{MHz}$, $\delta_1 = -2\pi \times 27.5\,\text{MHz}$, $\delta_2 = 2\pi \times 80\,\text{MHz}$, and $B = 10^{-4}\,\text{T}$. We feed the OBE with the raw branching fraction $p = 0.9449$ from our experiments as a best first-order approximation to calculate systematic shifts. The results presented below are obtained for the sequence of the third experimental run displayed in the Fig. 3.

The photodetector dead time induces an underestimation of the counts accumulated during the N_b counting window. To estimate the systematic shift associated with the dead time $\tau_{\text{PM}} = 30 \pm 2$ ns of the detection chain (photomultiplier and photon counter), we use the time-dependent solution of the OBE to calculate the conditional probability q that, following a first detection event, another photoelectron is emitted within a τ_{PM} time window. Since we know that after the emission of a photon the ion is in the ground state, the probability q is given by the following expression:

$$q = 1 - \exp\left(-\int_0^{\tau_{PM}} \varepsilon A_{SP}\sigma_{PP}(t)dt\right), \qquad (1)$$

where A_{SP} is the transition probability for the $5s\,^2S_{1/2} \rightarrow 5p\,^2P_{1/2}$ transition and $\sigma_{PP}(t)$ is the level $5p\,^2P_{1/2}$ population at time t. By neglecting losses of more than one photon and the contribution of the background photons, the total number of undetected photons in the measurement of N_b photons is then qN_b. In the nominal experimental conditions of the third acquisition run $q = 8.4 \times 10^{-5}$. This underestimation of N_b induces a systematic shift of $(4.3^{+1.8}_{-1.5}) \times 10^{-6}$ on p (see Table I). The uncertainty is evaluated by assuming a (very conservative) relative uncertainty of 20% on Ω_1, the parameter that mostly affects this systematic shift.

The finite lifetime of the $4d\,^2D_{3/2}$ state and the finite duration of the sequence time windows modify the average number of photons detected in each measurement phase with respect to the ideal case (infinite lifetime, infinite detection, and preparation windows). We can identify two main physical mechanisms responsible for this shift: the state preparation errors and the imperfect shelving in the metastable state that ends up with the ion in the fluorescence cycle during a measurement window. By comparing the average photon numbers obtained by solving the OBE (that take into account the experimental window durations and the lifetime $\tau_D = 435(4)$ ms measured in Ref. [47]) with the ideal case we obtain an estimate of the systematic shift associated to these effects in our experimental conditions. The estimated contribution to the systematic shift that affects p is $(0.4^{-0.4}_{+1.9}) \times 10^{-6}$ (see Table I). As in the case of the effect of τ_{PM}, the uncertainty that affects this shift is evaluated by assuming a relative uncertainty of 20% on Ω_1, which is the parameter that mainly affects the shift.

The last class of systematic shifts that we estimate with the OBE are those induced by the imperfect extinctions of the two lasers. This shift is obtained by comparing the results of the OBE that describe the experiments with perfect extinction to the case in which the extinction ratio is fixed to -77 dB as measured in the experiment. The estimated contribution of the imperfect extinction to the systematic shift that affects p is $(1 \pm 1) \times 10^{-8}$ (see Table I), dominated by the repumping beam leaks.

It is interesting to note that some effects partially cancel because they affect in a similar (albeit not identical) way signal and background. As an example, this is the case for the errors due to the relaxation of the shelved electronic excitation during the measurement of N_b and N_b^B. The compensation is not perfect because the two measurements do not start with the ion in the same electronic state. However, the transient dynamics in a typical experiment only covers a small fraction of the respective acquisition windows.

Let us finally remark that a hypothetical correlated time-duration unbalance between the phases of N_b and N_b^B (dominant contribution) in the sequential acquisition, within the limits of our negative check (i.e., 8 ns), would originate a systematic shift on p of $\simeq \pm 2 \times 10^{-6}$.

The summary of systematic errors is reported in Table I. These errors are about two orders of magnitude smaller than the statistical uncertainty; the final result for the branching fraction p is then $p = 0.9449(5)$ [$B = 17.14(16)$].

IV. DISCUSSION

In this section we discuss how our experimental determination of B compares to other experimental results and theoretical calculations present in the literature. First, we compare in Fig. 5 the experimental determination of B obtained by Gallagher [22] with our result. As in the case of Ca^+ studied in Ref. [10], there is no agreement between our data and Gallagher's experiments (performed in an argon discharge).

We can also compare these results to the theoretical estimates of $B = A_{SP}/A_{PD}$ that can be obtained starting from the calculated transition probabilities. The three points on the bottom of Fig. 5 (open symbols) have been calculated (with their error bars, whenever applicable) starting from data in Refs. [5,32,33]. As outlined in Ref. [32], there is no agreement between recent theoretical calculations and the experimental determination of B by Gallagher. This contrasts with the present experimental determination that is indeed compatible, within the smaller error bar, with the calculations of Refs. [5,32].

By using the lifetime $\tau_P = 7.39(7)$ ns measured by Pinnington and coworkers [24], the determinations of p can be also recast in terms of transition probabilities $A_{SP} = p/\tau_P$ and

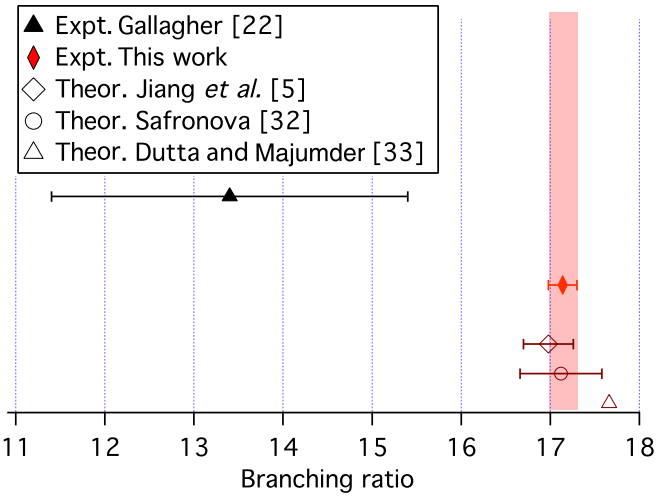

FIG. 5. Comparison of our measurement of the branching ratio B (filled diamond, red) with other experimental measurements or theoretical calculations. Vertical axis separation is used to offset the data from different works. The error bars (whenever present) represent the standard error associated to the determination of B. Reference [33] does not give information about standard error.

$A_{PD} = (1 - p)/\tau_P$. This is the strategy adopted in order to compile the NIST database [20,21] that takes advantage of the relatively small uncertainty on τ_P. In such a way it is possible to directly test the experimental determinations against the original quantities calculated in theoretical papers. In Fig. 6 we plot a compilation of the experimental determinations of A_{SP} and the theoretical calculations of the same quantity. All the determinations are compatible within the uncertainties attributed to measurements or calculations; let us note that the error bar associated to the present work is dominated by the uncertainty that affects τ_P. We included in this compilation the results of Ref. [25], even though the method for the

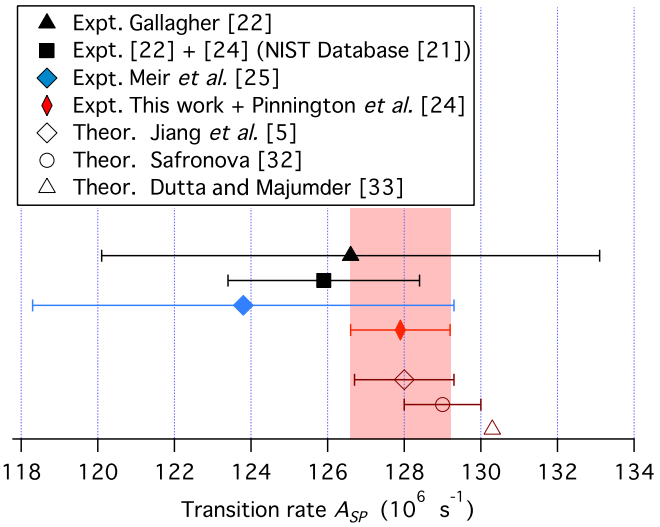

FIG. 6. Comparison of measurements and calculations of the transition probability A_{SP}. Vertical axis separation is used to offset different measurements. In this work we obtain $A_{SP} = 127.9(1.3) \times 10^6$ s^{-1}.

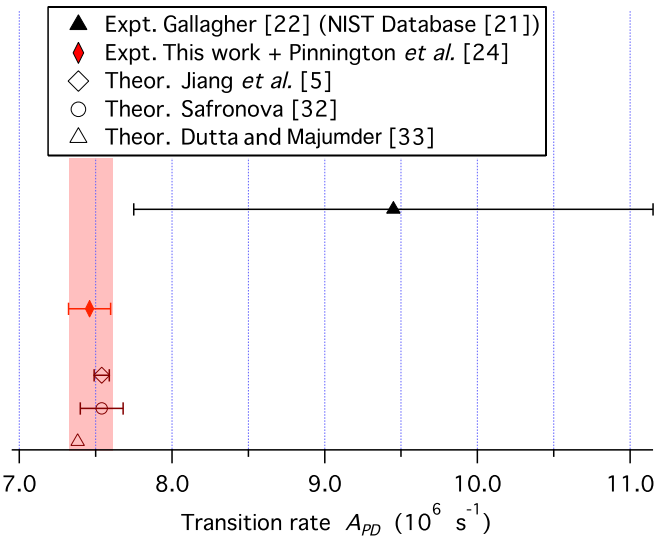

FIG. 7. Comparison of measurements and calculations of the transition probability A_{PD}. Vertical axis separation is used to offset different measurements. In this work we obtain $A_{PD} = 7.46(14) \times 10^6$ s^{-1}.

determination of A_{SP} was in this case quite indirect and the exact value of A_{SP} not crucial for their study.

In Fig. 7 we present the compilation concerning the transition probabilities A_{PD}. The error bar associated to the present work is in this case dominated by the uncertainty that affects B. It is interesting to note that our work brings back in agreement theory and experimental observations, in a similar way to what is discussed in Ref. [12] for $^{40}Ca^+$.

It is interesting to analyze the limitations of this method and the possible improvements that could reduce the uncertainty of the present result. Photon counting statistical uncertainty (dominated by the relatively low total number of photons detected during the N_r measurement phase) gives the largest contribution to our error bar. A longer acquisition time will obviously improve the precision of the measurement. Another effective approach is to increase the number of ions addressed in the experiment and/or the collection efficiency [11]. With this approach the systematic shift induced by the detector dead time may become larger than the statistical error and then a careful characterization of the detection chain is compulsory [15]. An effective way to mitigate this problem is to introduce more phases in the sequences in which the Rabi frequency Ω_1 is increased by steps [11]. Systematic shift uncertainty could in any case eventually limit the precision of the measurement of p.

We used our approach based on the solution of the OBE to reduce the systematic shift in the third experimental run down to a target value of $\simeq 5 \times 10^{-6}$ (i.e., two orders of magnitudes lower than our statistical error). The measured dead time of the detection chain gives a systematic shift on p of 4.3×10^{-6} for our nominal driving lasers parameters ($\Omega_1 = 2\pi \times 8.7$ MHz, $\Omega_2 = 2\pi \times 18$ MHz, $\delta_1 = -2\pi \times 27.5$ MHz, $\delta_2 = 2\pi \times 80$ MHz, and $B = 10^{-4}$ T). This systematic shift increases with Ω_1 as shown in Fig. 8. On the other hand the systematic shift on p induced by the finite lifetime of the $4d\,^2D_{3/2}$ state and the finite duration of the sequence time windows can be reduced by increasing the N_b measurement-window

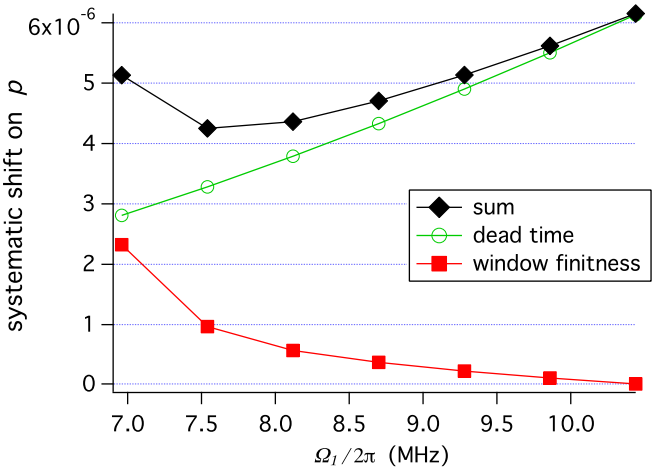

FIG. 8. Systematic shifts affecting p as a function of the Rabi frequency of the cooling laser Ω_1 as calculated solving the OBE for the sequence presented in Fig. 3. Red filled squares: contribution induced by the finite lifetime of the $4d\,^2D_{3/2}$ state and the finite duration of the sequence time windows. Green open circles: contribution induced by the dead time of the photodetection chain. Black filled diamonds: sum of the two contributions.

duration. We fixed this window duration at 160 μs such that its contribution to the systematic shift becomes lower than the contribution of dead time (lower curve of Fig. 8). It is interesting to note that with these parameters these two contributions to the systematic shift have an opposite slope as a function of Ω_1. This introduces some extra robustness against the fluctuations of this parameter that maximally affect the systematic shift uncertainty (sum of the contributions, upper curve of Fig. 8). Such a kind of optimization could be adapted to multi-ion and multi-intensity experiments in order to minimize the contribution of the systematic shift uncertainty.

In conclusion we measured the branching fractions for the decay of the $5p\,^2P_{1/2}$ state of $^{88}Sr^+$: the probabilities p and $1-p$ for the decay of the $5p\,^2P_{1/2}$ to the $5s\,^2S_{1/2}$ and $4d\,^2D_{3/2}$ states are, respectively, $p = 0.9449(5)$ and $0.0551(5)$, with a fractional uncertainty on p of 5×10^{-4}. In terms of branching ratio the result is $B = 17.14(16)$, affected by a fractional uncertainty of 1×10^{-2}. This result can be compared to previous experimental determinations and to theoretical calculations: when considering the branching ratio and the transition probability A_{PD} our work brings back in agreement theory and experimental observations and constitutes an important check for the validity of recent theories. Finally, this experiment demonstrates the applicability of microtrap technology in the domain of precision measurements and spectroscopy.

ACKNOWLEDGMENTS

We thank A. Anthore for enlighting discussions concerning trap fabrication; C. Manquest and S. Suffit for their help in cleanroom processes; and M. Apfel, P. Lepert, and M. Nicolas for technical support. We also thank B. Szymanski for fruitful discussions and help in the early stages of the experiment. This study was partly founded by Conseil Régional, Île-de-France through the DIM Nano-k (projects DEQULOT and EXPLOR@ION). V.T. thanks the Ecole Normale Supérieure de Lyon for financial support in the form of a fourth year study project.

[1] M. S. Safronova and W. R. Johnson, in *Advances In Atomic, Molecular, and Optical Physics*, edited by P. R. B. Ennio Arimondo and C. C. Lin (Academic, New York, 2008), Vol. 55, pp. 191–233.
[2] C. S. Wood, S. C. Bennett, D. Cho, B. P. Masterson, J. L. Roberts, C. E. Tanner, and C. E. Wieman, Science **275**, 1759 (1997); J. Ginges and V. Flambaum, Phys. Rep. **397**, 63 (2004).
[3] M. A. Bautista, T. R. Gull, K. Ishibashi, H. Hartman, and K. Davidson, Mon. Not. R. Astron. Soc. **331**, 875 (2002).
[4] H. S. Margolis, Contemp. Phys. **51**, 37 (2010).
[5] D. Jiang, B. Arora, M. S. Safronova, and C. W. Clark, J. Phys. B **42**, 154020 (2009).
[6] R. Blatt and D. Wineland, Nature (London) **453**, 1008 (2008).
[7] D. J. Wineland, C. Monroe, W. M. Itano, D. Leibfried, B. E. King, and D. M. Meekhof, J. Res. Natl. Inst. Stand. Technol. **103**, 259 (1998).
[8] H. Häffner, C. Roos, and R. Blatt, Phys. Rep. **469**, 155 (2008).
[9] P. A. Barton, C. J. S. Donald, D. M. Lucas, D. A. Stevens, A. M. Steane, and D. N. Stacey, Phys. Rev. A **62**, 032503 (2000).
[10] R. Gerritsma, G. Kirchmair, F. Zähringer, J. Benhelm, R. Blatt, and C. F. Roos, Eur. Phys. J. D **50**, 13 (2008).
[11] M. Ramm, T. Pruttivarasin, M. Kokish, I. Talukdar, and H. Häffner, Phys. Rev. Lett. **111**, 023004 (2013).
[12] M. Hettrich, T. Ruster, H. Kaufmann, C. F. Roos, C. T. Schmiegelow, F. Schmidt-Kaler, and U. G. Poschinger, Phys. Rev. Lett. **115**, 143003 (2015).
[13] N. Kurz, M. R. Dietrich, G. Shu, R. Bowler, J. Salacka, V. Mirgon, and B. B. Blinov, Phys. Rev. A **77**, 060501 (2008).
[14] C. Auchter, T. W. Noel, M. R. Hoffman, S. R. Williams, and B. B. Blinov, Phys. Rev. A **90**, 060501 (2014).
[15] D. De Munshi, T. Dutta, R. Rebhi, and M. Mukherjee, Phys. Rev. A **91**, 040501 (2015).
[16] H. S. Margolis, G. P. Barwood, G. Huang, H. A. Klein, S. N. Lea, K. Szymaniec, and P. Gill, Science **306**, 1355 (2004).
[17] G. P. Barwood, H. S. Margolis, G. Huang, P. Gill, and H. A. Klein, Phys. Rev. Lett. **93**, 133001 (2004).
[18] V. Letchumanan, M. A. Wilson, P. Gill, and A. G. Sinclair, Phys. Rev. A **72**, 012509 (2005).
[19] W. E. Lybarger, J. C. Berengut, and J. Chiaverini, Phys. Rev. A **83**, 052509 (2011).
[20] D. P. J. E. Sansonetti, J. Phys. Chem. Ref. Data **41**, 013102 (2012).
[21] A. Kramida, Y. Ralchenko, J. Reader, and NIST-ASD-Team (2015), National Institute of Standards and Technology, Gaithersburg, MD.
[22] A. Gallagher, Phys. Rev. **157**, 24 (1967).

[23] P. Kuske, N. Kirchner, W. Wittmann, H. Andrä, and D. Kaiser, Phys. Lett. A **64**, 377 (1978).
[24] E. H. Pinnington, R. W. Berends, and M. Lumsden, J. Phys. B **28**, 2095 (1995).
[25] Z. Meir, O. Schwartz, E. Shahmoon, D. Oron, and R. Ozeri, Phys. Rev. Lett. **113**, 193002 (2014).
[26] A. A. Madej, J. E. Bernard, P. Dubé, L. Marmet, and R. S. Windeler, Phys. Rev. A **70**, 012507 (2004).
[27] CIPM, Recommendation 1 (CI-2006), International Committee for Weights and Measures, report of the 95th meeting, 2006 (unpublished).
[28] M. Poirier, Zeitschrift für Physik D **25**, 117 (1993).
[29] E. Biémont, J. Lidberg, S. Mannervik, L.-O. Norlin, P. Royen, A. Schmitt, W. Shi, and X. Tordoir, Eur. Phys. J. D **11**, 355 (2000).
[30] B. K. Sahoo, M. R. Islam, B. P. Das, R. K. Chaudhuri, and D. Mukherjee, Phys. Rev. A **74**, 062504 (2006).
[31] J. Mitroy, J. Y. Zhang, and M. W. J. Bromley, Phys. Rev. A **77**, 032512 (2008).
[32] U. I. Safronova, Phys. Rev. A **82**, 022504 (2010).
[33] N. N. Dutta and S. Majumder, Phys. Rev. A **90**, 012522 (2014).
[34] J. Chiaverini, R. B. Blakestad, J. Britton, J. D. Jost, C. Langer, D. Leibfried, R. Ozeri, and D. J. Wineland, Quantum Inf. Comput. **5**, 419 (2005).
[35] D. T. C. Allcock, J. A. Sherman, D. N. Stacey, A. H. Burrell, M. J. Curtis, G. Imreh, N. M. Linke, D. J. Szwer, S. C. Webster, A. M. Steane *et al.*, New J. Phys. **12**, 053026 (2010).
[36] M. G. House, Phys. Rev. A **78**, 033402 (2008).
[37] D. J. Berkeland, J. D. Miller, J. C. Bergquist, W. M. Itano, and D. J. Wineland, J. Appl. Phys. **83**, 5025 (1998).
[38] S. Removille, R. Dubessy, Q. Glorieux, S. Guibal, T. Coudreau, L. Guidoni, and J.-P. Likforman, Appl. Phys. B **97**, 47 (2009); E. Kirilov and S. Putterman, Eur. Phys. J. D **54**, 683 (2009).
[39] A. Madej, L. Marmet, and J. Bernard, Appl. Phys. B **67**, 229 (1998); A. G. Sinclair, M. A. Wilson, and P. Gill, Opt. Commun. **190**, 193 (2001).
[40] A. Shiner, A. Madej, P. Dubé, and J. Bernard, Appl. Phys. B **89**, 595 (2007).
[41] J. H. T. Burke, O. Garcia, K. J. Hughes, B. Livedalen, and C. A. Sackett, Rev. Sci. Instrum. **76**, 116105 (2005).
[42] N. Seymour-Smith, P. Blythe, M. Keller, and W. Lange, Rev. Sci. Instrum. **81**, 075109 (2010).
[43] B. Dubost, R. Dubessy, B. Szymanski, S. Guibal, J.-P. Likforman, and L. Guidoni, Phys. Rev. A **89**, 032504 (2014).
[44] D. J. Berkeland and M. G. Boshier, Phys. Rev. A **65**, 033413 (2002).
[45] A. Gardner, K. Sheridan, W. Groom, N. Seymour-Smith, and M. Keller, Appl. Phys. B **117**, 755 (2014).
[46] I. Siemers, M. Schubert, R. Blatt, W. Neuhauser, and P. E. Toschek, Europhys. Lett. **18**, 139 (1992).
[47] S. Mannervik, J. Lidberg, L.-O. Norlin, P. Royen, A. Schmitt, W. Shi, and X. Tordoir, Phys. Rev. Lett. **83**, 698 (1999).
[48] G. Grynberg, A. Aspect, and C. Fabre, *Introduction to Quantum Optics: From the Semi-Classical Approach to Quantized Light*, 1st ed. (Cambridge University, Cambridge(UK), 2010).